CALPHAD: Computer Coupling of Phase Diagrams and Thermochemistry 35 (2011) 523–532

Contents lists available at SciVerse ScienceDirect

CALPHAD: Computer Coupling of Phase Diagrams and Thermochemistry

journal homepage: www.elsevier.com/locate/calphad

Thermodynamic optimization of the Li–Mg and Al–Li–Mg systems

Peisheng Wang [a], Yong Du [a,b,*], Shuhong Liu [a]

[a] State Key Laboratory of Powder Metallurgy, Central South University, Changsha, Hunan, 410083, PR China

[b] Science Center for Phase Diagram & Materials Design and Manufacture, Central South University, Changsha, Hunan, 410083, PR China

ARTICLE INFO

Article history:
Received 26 June 2011
Received in revised form
8 September 2011
Accepted 9 September 2011
Available online 6 October 2011

Keywords:
Phase diagram
Magnesium alloys
Thermodynamic modeling
CALPHAD

ABSTRACT

The thermodynamic reassessment of the Li–Mg system has been performed by considering the latest experimental data. A noticeable improvement for the description of the experimental phase diagram and thermodynamic data has been made in the present description of the Li–Mg system compared with the previous assessments. The artificial phase equilibria, which exist in the previous optimization, have been eliminated. The obtained thermodynamic description for the Li–Mg system is then combined with those for the Al–Mg and Al–Li systems to form a basis for a ternary assessment. A set of self-consistent thermodynamic parameters for the Al–Li–Mg system is then obtained. Comparisons between the calculated and experimental results in the Al–Li–Mg system show that the present description can account for the experimental data satisfactorily.

1. Introduction

It has been a conventional wisdom that to reduce weight is an urgent need in transport industry because of the significant economic benefits, especially the fuel economy. As the lightest structure materials, the Li–Mg based alloys have attracted wide interest. For example, LA141 (Mg–14Li–1Al, wt%) is the most widely used Li–Mg based alloy due to its superior plasticity and ductility [1,2]. Besides, the Al–Li–Mg system is also the basis of some multicomponent aluminum alloys and lithium battery materials. For example, the 1420 aluminum alloys, which are based on the Al–Li–Mg system, have the similar corrosion resistances of the 5*xxx* series aluminum alloys, but much higher strengths [3].

The phase equilibria and thermodynamics of the Al–Li–Mg system are critical information to improve the properties of these alloys and develop new series of materials. However, due to the high reactivity of lithium, it is difficult to prepare alloys to investigate the phase equilibria in the Li-rich corner. Thus a through CALPHAD (CALculation of PHAse Diagram) modeling based on all available phase equilibrium data and thermodynamic data is preferable since the phase equilibria of the Al–Li–Mg system on the entire composition and temperature ranges can be attained by means of CALPHAD technique. The thermodynamic optimization of the Al–Li–Mg system has been performed by Dubost et al. [4], who only considered the experimental data in the Al-rich region. Another drawback is that the binary phase diagrams used by Dubost et al. [4] are different from the widely accepted ones. Thus a comprehensive thermodynamic assessment of this ternary is necessary.

The objective of the present work is to provide a thermodynamic description for the Al–Li–Mg system in the entire composition and temperature ranges. The sub-binary systems are evaluated first in order to provide the accurate thermodynamic description for each binary system.

2. Literature review

2.1. The Li–Mg system

The thermodynamic parameters of the Al–Li and Al–Mg systems have been well established by Saunders [5,6], while a reassessment of the Li–Mg system is necessary.

The Li–Mg system has been optimized by three groups of researchers [6–8]. Saunders [6] first optimized the Li–Mg system based on the assessment of Nayeb et al. [9]. However, the latest liquidus and solidus measured by Schürmann and Voss [10] were taken into account by Saunders [6] nor Nayeb et al. [9]. The noticeable deviations between the calculated phase diagram [6] and the experimental data [10] are shown in Fig. 1(a). Later, Gasior et al. [7] re-optimized the Li–Mg system taking into account their own data and all the experimental data from the literature. However, the calculated phase diagram cannot reproduce the experimental results well. Besides, some artificial phase relations appear in the Li-rich corner at about 80 °C, as shown in Fig. 1(b).

* Corresponding author at: State Key Laboratory of Powder Metallurgy, Central South University, Changsha, Hunan, 410083, PR China. Tel.: +86 731 88836213; fax: +86 731 88710855.
E-mail address: yongducalphad@gmail.com (Y. Du).

0364-5916/$ – see front matter © 2011 Elsevier Ltd. All rights reserved.
doi:10.1016/j.calphad.2011.09.003

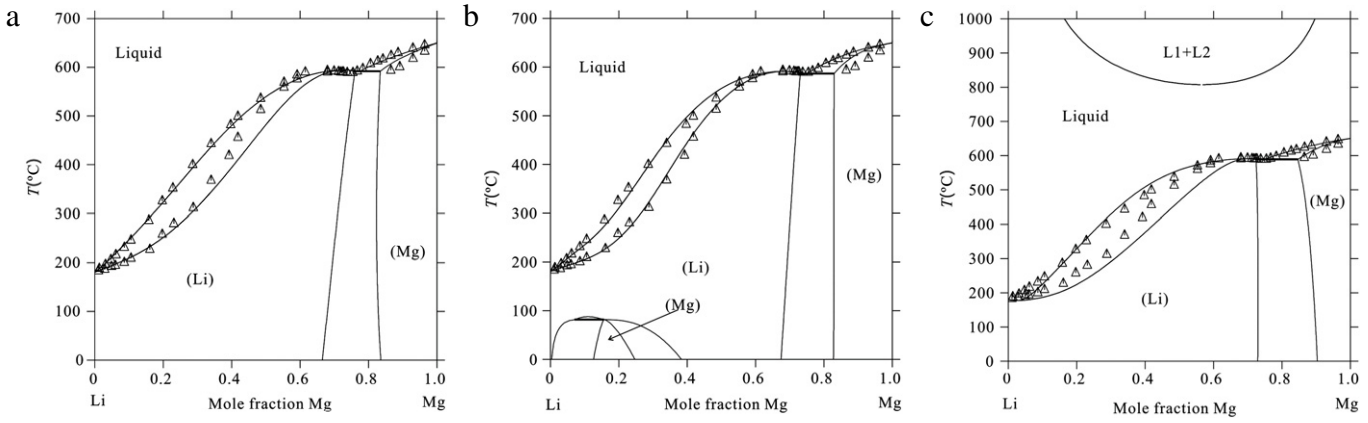

Fig. 1. Calculated Li–Mg phase diagram using the parameters from the literature compared with the experimental data [10] (a) Saunders [6] (b) Gasior et al. [7] (c) Braga et al. [8].

Braga et al. [8] re-assessed this binary system based on the results of Saunders [6]. As shown in Fig. 1(c), there are at least three drawbacks: (i) the calculated phase diagram of Braga et al. [8] shows a great deviation from the experimental one in the Li-rich part; (ii) an inverse liquid miscibility gap emerges above 700 °C; (iii) a congruent melting point appears in the calculated phase diagram at the Li rich side, which is against the experimental results. Consequently, a re-assessment of the Li–Mg system is necessary.

The present work is based on the assessment of Gasior et al. [7]. The following data were utilized in the present work: the liquidus and solidus data within the entire composition range from Schürmann and Voss [10], the solvus of the (Mg) phase from Refs. [7,10–12], the solvus of the (Li) phase from Refs. [11,13], the enthalpies of mixing for liquid phases by Sommer [14] and the activities of (Li) determined by various researchers [7,15,16].

2.2. The Al–Li–Mg system

The phase equilibria and the thermodynamic properties of the Al–Li–Mg system have been reviewed by Ghosh [17] and are updated in this work. Table 1 lists the crystallographic data for the solid phases in the Al–Li–Mg system [17–19].

The liquidus surface projection and the invariant reactions associated with the liquid phase have been measured by Shamray [20], Drits et al. [21], Schürmann and Voss [10] and Dubost et al. [4]. The results of Shamray [20] and Drits et al. [21] show great discrepancies from the widely accepted sub-binary phase diagrams. Thus, the experimental data of Shamray [20] and Drits et al. [21] were not accepted presently. Due to the high evaporability and reactivity of both Li and Mg, Schürmann and Voss [10] designed a special equipment to prepare the Al–Li–Mg alloys [10]. They investigated the system in the entire composition range using X-ray diffraction (XRD), optical metallography (OM) and electron probe microanalysis (EPMA). In general, the experimental results of Schürmann and Voss [10] are accepted. However, two modifications have been made in order to keep consistent with the presently accepted sub-binary phase diagrams [5,6]. (i) As ζ phase ($Al_{11}Mg_{10}$) observed by Schürmann and Voss [10] is not considered as a stable phase in the accepted Al–Mg phase diagram [5], two invariant reactions associated with ζ : U_7 ($L + \gamma = \zeta + \beta$) and U_8 ($L + \zeta = \varepsilon + \beta$), in [10] are not accepted in the present work. (ii) Al_4Li_9 phase which is not present in the previous proposed liquidus surface projection [10], is included in the present work. Allowing for this, the liquidus data at the Li-rich corner were given lower weight in the optimization. Dubost et al. [4] determined three invariant reactions in the Al-rich corner. The first two are consistent with the results of Schürmann and Voss [10]. For the last one, the invariant reaction determined by Dubost et al. [4] is a eutectic reaction $L = (Al) + \beta + \gamma$, while the experimental results of Schürmann and Voss [10] suggest a transition reaction of $L + (Al) = \beta + \gamma$. It is difficult to judge which experimental result is right. As has been mentioned above, this invariant reaction type can be judged by a comprehensive thermodynamic calculation.

The isothermal sections have been measured several times [11,20–27]. The phase relations determined by various authors [11,20–27] were consistent with each other. However, most of the researches [11,20–26] failed to determine the compositions of the equilibrium phases except the latest one by Schürmann and Geissler [27]. The isothermal sections below 60 at.% Li at 200, 300 and 400 °C were measured by Schürmann and Geissler [27], who prepared 178 alloys in a specially designed vacuum induction furnace. The alloys were annealed at each specified temperature for 260 h and quenched in water or oil. OM and EPMA were employed for phase identifications and composition measurements. The phase equilibrium data due to Schürmann and Geissler [27] were utilized in the present optimization with higher weights.

Two ternary compounds, τ and τ_1, have been reported in the Al–Li–Mg system. The τ phase was found by Shamray [20], Shamray and Kurnakov [28], and its existence was confirmed by several groups of researchers [23,24,26,27,29]. This phase was previously reported to be a stoichiometric phase Al_2LiMg [20,23,24,28,29]. However, recent results [26,27] suggested that it has a slight homogeneity range of 32.0–34.2 at.% Li and 13.5–14.0 at.% Mg. Such a homogeneity range is far from the stoichiometry Al_2LiMg. The experimental results [26,27] were taken into account in the present optimization. The previously reported τ_1 phase [11,22] was not confirmed by the subsequent researchers. This phase could be a metastable phase as observed by Weinberg et al. [23] and Nikulin et al. [30]. Consequently, it is not considered in the present work.

Moser et al. [31] determined the enthalpies of mixing of liquid phases in the temperature range of 596–758 °C using an isothermal high temperature mixing calorimeter. These data [31] were used for the present optimization.

Generally speaking, due to the high evaporability and high reactivity of both Li and Mg, it is difficult to investigate this ternary system using conventional methods and equipments. In fact, the experimental investigations of the ternary system were limited to the Mg-corner or the Al-corner until Schürmann and his coworkers developed a special designed equipment to prepare alloys. Consequently, most of the results from Schürmann and his coworkers [10] were accepted in the present optimization.

Table 1
Crystallographic data for the solid phases in the Al–Li–Mg system [17–19].

Phase/temperature range (°C)	Person symbol/prototype	Space group	Lattice parameter (pm)	Ref.
(Al) ≤ 660.45	cF4 Cu	*Fm*3 m	$a = 404.88$	[17]
(Li) ≤ 180.60	*cI*2 *W*	*Im*3 m	$a = 351.0$	[17]
(Mg) ≤ 650	*hP*2 Mg	*P*63/mmc	$a = 320.89$ $c = 521.01$	[17]
AlLi ≤ 700	*cF* 16 NaTl	*Fd*3 m	$a = 637.0$	[18]
Al_2Li_3 ≤ 520	*hR*15 Bi_2Te_3	*Fd*3 m	$a = 450.8$ $c = 1426.0$	[18]
Al_4Li_9 330–275	*mC*26 Al_4Li_9	*C*2/m	$a = 1915.51$ $b = 542.88$ $c = 449.88$ $\beta = 107.67°$	[18]
β, Al_3Mg_2 ≤ 452	*cF* 1168 Al_3Mg_2	*Im* − 3 m	$a = 2816$–2824	[19]
γ, $Mg_{17}Al_{12}$ ≤ 458	*cI*58 αMn	*P*4$_1$32	$a = 1054.38$	[19]
ε, $Mg_{30}Al_{23}$ 410–250 τ	*hR*159 $Mn_{44}Si_9$ *c**456	*R*3	$a = 1282.54$ $c = 2174.78$ $a = 2031.0$	[19] [17]

3. Thermodynamic modeling

3.1. Pure elements

The Gibbs energy functions for pure elements Al, Li and Mg are taken from the Scientific Group Thermodata Europe (SGTE) compiled by Dinsdale [32].

3.2. Sub-binary systems

3.2.1. Li–Mg system

The (Li) phase and (Mg) phase are modeled as Bcc_A2 and Hcp_A3, respectively. The excess Gibbs energy of the liquid phase, (Mg) phase, (Li) phase are described by the Redlich–Kister (R–K) polynomial [33] as Eq. (1)

$$^{ex}G_m^L = x(1-x)\sum_{i=0}^{n} {}^iL(1-2x)^i \quad (1)$$

in which $^iL = A_i + B_i \cdot T$ are the parameters to be optimized.

3.2.2. Al–Li and Al–Mg systems

The thermodynamic parameters of the binary systems Al–Mg and Al–Li are taken from Refs. [5,34], respectively. The calculated Al–Li and Al–Mg phase diagrams are shown in Figs. 2 and 3, respectively.

3.3. Al–Li–Mg system

3.3.1. Solution phases

The solution phases: liquid, (Mg), (Li) and (Al), are described by the substitutional solution model. The (Al) phase is modeled as Fcc_A1. The molar Gibbs energy of the solution phase is described as

$$^0G_m^\Phi = x_{Al} \cdot {}^0G_{Al}^\Phi + x_{Li} \cdot {}^0G_{Li}^\Phi + x_{Mg} \cdot {}^0G_{Mg}^\Phi + R \cdot T(x_{Al} \cdot \ln x_{Al} + x_{Li} \cdot \ln x_{Li} + x_{Mg} \cdot \ln x_{Mg}) + {}^{ex}G_m^\Phi \quad (2)$$

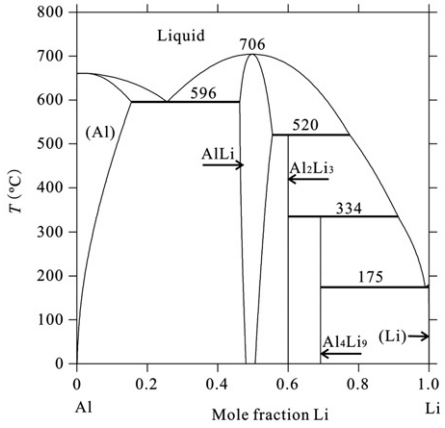

Fig. 2. Calculated Al–Li phase diagram [5].

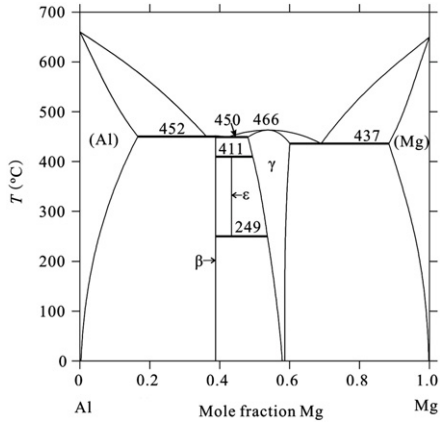

Fig. 3. Calculated Al–Mg phase diagram [6].

in which R is the gas constant, and x_{Al} x_{Li} and x_{Mg} are the molar fractions of Al, Li and Mg, respectively. The standard element

reference (SER) state, the stable structure of the element at 298.15 K and 1 bar, is used as the reference state of the Gibbs energy. ${}^{ex}G_m^{\Phi}$ is the excess Gibbs energy of the phase, which can be described by the R–K polynomial [33]:

$$ {}^{ex}G_m^{\Phi} = x_{Al}\cdot x_{Li}\cdot L_{Al,Li}^{\Phi} + x_{Al}\cdot x_{Mg}\cdot L_{Al,Mg}^{\Phi} + x_{Li}\cdot x_{Mg}\cdot L_{Li,Mg}^{\Phi} + x_{Al}\cdot x_{Li}\cdot x_{Mg}\cdot L_{Al,Li,Mg}^{\Phi} \quad (3) $$

in which $L_{Al,Li}^{\Phi}L_{Al,Mg}^{\Phi}$ and $L_{Li,Mg}^{\Phi}$ are parameters from the sub-binary systems, $L_{Al,Li,Mg}^{\Phi}$ is the ternary parameter and can be described as

$$ L_{Al,Li,Mg}^{\Phi} = x_{Al}\cdot{}^{0}L_{Al,Li,Mg}^{\Phi} + x_{Li}\cdot{}^{1}L_{Al,Li,Mg}^{\Phi} + x_{Mg}\cdot{}^{2}L_{Al,Li,Mg}^{\Phi}. \quad (4) $$

3.3.2. Binary phases extending into ternary system

The sublattice model [35] was used to describe the β, γ, Al_2Li_3 and AlLi phase. The β phase and the Al_2Li_3 phase are stoichiometric compounds in the Al–Mg and Al–Li binary systems, respectively. According to the experimental data [27], it is reasonable to assume that the Li atoms only substitute for the Mg atoms in the β phase, while the Mg atoms only substitute for the Li atoms in the Al_2Li_3 phase. Consequently, the β and Al_2Li_3 phases are modeled with the sublattice models $Al_{140/229}(Mg, Li)_{89/229}$ and $(Al, Mg)_{0.4}Li_{0.6}$, respectively.

Since the solubility of Li in γ phase is considerable (17.7 at.% at 400 °C), and the content of Al is not affected by the addition of Li, it is assumed that Li atoms only replace the Mg atoms in the first sublattice of the γ phase. In the binary Al–Mg system, the γ phase is modeled as $Mg_{10/58}(Al, Mg)_{24/58}(Al, Mg)_{24/58}$. Consequently, the γ phase is modeled with a three-sublattice model $(Li, Mg)_{10/58}(Al, Mg)_{24/58}(Al, Mg)_{24/58}$ in the ternary system. The elements in bold are the major species in the corresponding sublattices.

In the binary Al–Li system, the AlLi phase is modeled as $(Al, Li)_{0.5}(Li, Va)_{0.5}$. In view of the large solubility of Mg in AlLi phase, this phase is modeled with the sublattice model $(Al, Li, Mg)_{0.5}(Li, Mg, Va)_{0.5}$.

Taking the γ phase for example, its Gibbs energy function is described by the following equation:

$$\begin{aligned} G_m^{\gamma} - H^{SER} &= y'_{Li}y''_{Al}y'''_{Al}{}^{0}G^{\gamma}_{Li:Al:Al} + y'_{Li}y''_{Al}y'''_{Mg}{}^{0}G^{\gamma}_{Li:Al:Mg} \\ &+ y'_{Li}y''_{Mg}y'''_{Al}{}^{0}G^{\gamma}_{Li:Mg:Al} + y'_{Li}y''_{Mg}y'''_{Mg}{}^{0}G^{\gamma}_{Li:Mg:Mg} \\ &+ y'_{Mg}y''_{Al}y'''_{Al}{}^{0}G^{\gamma}_{Mg:Al:Al} + y'_{Mg}y''_{Al}y'''_{Mg}{}^{0}G^{\gamma}_{Mg:Al:Mg} \\ &+ y'_{Mg}y''_{Mg}y'''_{Al}{}^{0}G^{\gamma}_{Mg:Mg:Al} + y'_{Mg}y''_{Mg}y'''_{Al}{}^{0}G^{\gamma}_{Mg:Mg:Al} \\ &+ 10/58\cdot R\cdot T(y'_{Li}\ln y'_{Li} + y'_{Mg}\ln y'_{Mg}) \\ &+ 24/58\cdot R\cdot T(y''_{Al}\ln y''_{Al} + y''_{Mg}\ln y''_{Mg}) \\ &+ 24/58\cdot R\cdot T(y'''_{Al}\ln y'''_{Al} + y'''_{Mg}\ln y'''_{Mg}) \\ &+ y'_{Li}y'_{Mg}(y''_{Mg}y'''_{Al}L^{MgNi_2}_{Li,Mg:Mg:Al} + y''_{Al}y'''_{Al}L^{MgNi_2}_{Li,Mg:Al:Al} \\ &+ y''_{Mg}y'''_{Mg}L^{MgNi_2}_{Li,Mg:Mg:Mg} + y''_{Al}y'''_{Mg}L^{MgNi_2}_{Li,Mg:Al:Mg}) \\ &+ y''_{Mg}y''_{Al}(y'_{Mg}y'''_{Al}L^{MgNi_2}_{Mg:Al,Mg:Al} \\ &+ y'_{Mg}y'''_{Mg}L^{MgNi_2}_{Mg:Al,Mg:Mg} + y'_{Li}y'''_{Al}L^{MgNi_2}_{Li:Al,Mg:Al} + y'_{Li}y'''_{Mg}L^{MgNi_2}_{Li:Al,Mg:Mg}) \\ &+ y'''_{Al}y'''_{Mg}(y'_{Mg}y''_{Al}L^{MgNi_2}_{Mg:Al:Al,Mg} + y'_{Mg}y''_{Mg}L^{MgNi_2}_{Mg:Mg:Al,Mg} \\ &+ y'_{Li}y''_{Al}L^{MgNi_2}_{Li:Al:Al,Mg} + y'_{Li}y''_{Mg}L^{MgNi_2}_{Li:Mg:Al,Mg}). \end{aligned} \quad (5)$$

3.3.3. The ternary phase τ

Considering the crystal structure of τ phase is unknown and its composition range is from 32.0 to 34.2 at.% Li and 13.5 to 14.0 at.% Mg, this ternary phase τ is modeled as the stoichiometric compound $Al_{53}Li_{33}Mg_{14}$. The Gibbs energy of the ternary phase τ is described as

$$ G_{\tau} - H^{SER} = 0.53\cdot{}^{0}G_{Al}^{(Al)} + 0.33\cdot{}^{0}G_{Li}^{(Li)} + 0.14\cdot{}^{0}G_{Mg}^{(Mg)} + \Delta G_f^{\tau} \quad (6) $$

in which H^{SER} is the abbreviation of $0.53\cdot H_{Al}^{SER} + 0.33\cdot H_{Li}^{SER} + 0.14\cdot H_{Mg}^{SER}$ and $\Delta G_f^{\tau} = A + B\cdot T$ represents the Gibbs energy of formation of the compound τ. The parameters A and B are to be optimized.

4. Results and discussion

The optimization of the Li–Mg and Al–Li–Mg systems was carried out by the PARROT program [36]. The step-by-step optimization procedure described by Du et al. [37] was utilized in the present assessment. The Li–Mg system was optimized first. The obtained thermodynamic description for the Li–Mg system was then combined with those for the Al–Mg and Al–Li systems to form a basis for a ternary assessment. To prevent the occurrence of the artificial phase relations in the Li–Mg and Al–Li–Mg systems, some thermodynamic constraints have been added during the optimization, as discussed in detail by Wang et al. [38].

4.1. The Li–Mg system

The optimized parameters are listed in Table 2. It should be mentioned here that, the parameters ${}^{0}L_{Li,Va:Va}^{(Li)}$ and ${}^{0}L_{Mg,Va:Va}^{(Li)}$ are assessed with a very large value of 350,000 in the present work. If a smaller value, for example 100,000, is evaluated to these two parameters, the driving force of (Li) phase at 2000 °C will become a positive value, which is obviously incorrect. Thus a value as large as 350,000 for both ${}^{0}L_{Li,Va:Va}^{(Li)}$ and ${}^{0}L_{Mg,Va:Va}^{(Li)}$ is necessary to avoid a series of possible problems. Fig. 4 shows the calculated Li–Mg phase diagram using the presently obtained parameters. As presented in Fig. 4(a), the present calculation can reproduce the experimental data reasonably except for the Mg solidus. In the present work, we have tried to use ${}^{0}L_{Li,Mg:Va}^{(Mg)}$, ${}^{1}L_{Li,Mg:Va}^{(Mg)}$ and ${}^{2}L_{Li,Mg:Va}^{(Mg)}$ to describe the excess Gibbs energy of the (Mg) phase. However, almost no improvement can be obtained in comparison with the use of ${}^{0}L_{Li,Mg:Va}^{(Mg)}$ and ${}^{1}L_{Li,Mg:Va}^{(Mg)}$. The inverse miscibility gap and artificial phase relations in the Li-rich corner, which were found in the previous optimizations [7,8], are eliminated in the present work.

The reliability of the present calculation can be validated by comparing the calculated activities of Li in the three phases: liquid, (Li) and (Mg) with the experimental data. For the liquid phase, as shown in Fig. 5, the calculated activities of Li in liquid phase at various temperatures fit well with the experimental data. The superiority of the present calculation can be revealed by comparing the calculated activities of Li in the (Li) phase resulting from Saunders [6], Gasior et al. [7], Braga et al. [8] and present work, together with the experimental data [7,16], as shown in Fig. 6. The present calculation is the best description of the activity of Li in the (Li) phase. For the (Mg) phase, it has been pointed out by Gasior et al. [7], due to the self-titration of Li, the determined activities of Li in the dilute solutions are imprecise. So the activities of Li in the (Mg) phase were given lower weight in the present work. That is the reason for the noticeable deviations between the calculated activity of Li in the (Mg) phase and the experimental data, as shown in Fig. 7. An addition proof on the reliability of the present thermodynamic calculation is provided in Fig. 8, where the calculated enthalpy of mixing for the liquid phase at 667 °C is compared with the experimental values from Sommer [14]. It is demonstrated that these experimental data [14] are well fitted by the present thermodynamic calculation.

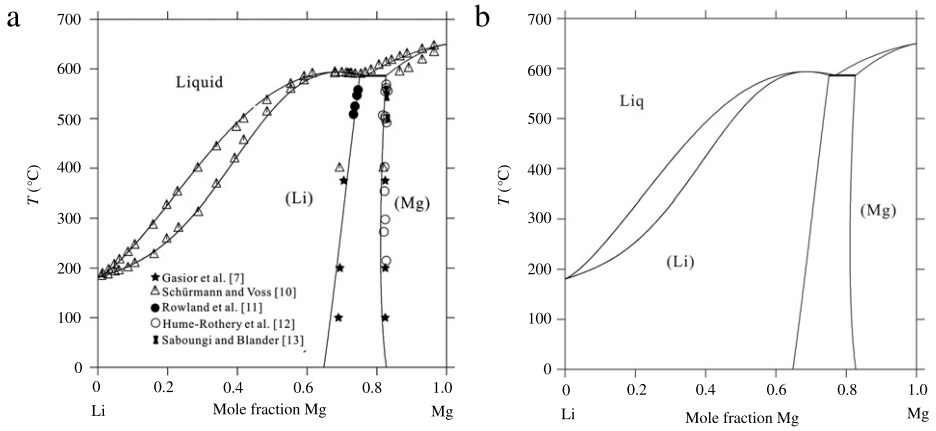

Fig. 4. The presently calculated Li–Mg phase diagram (a) with the experimental data (b) without the experimental data.

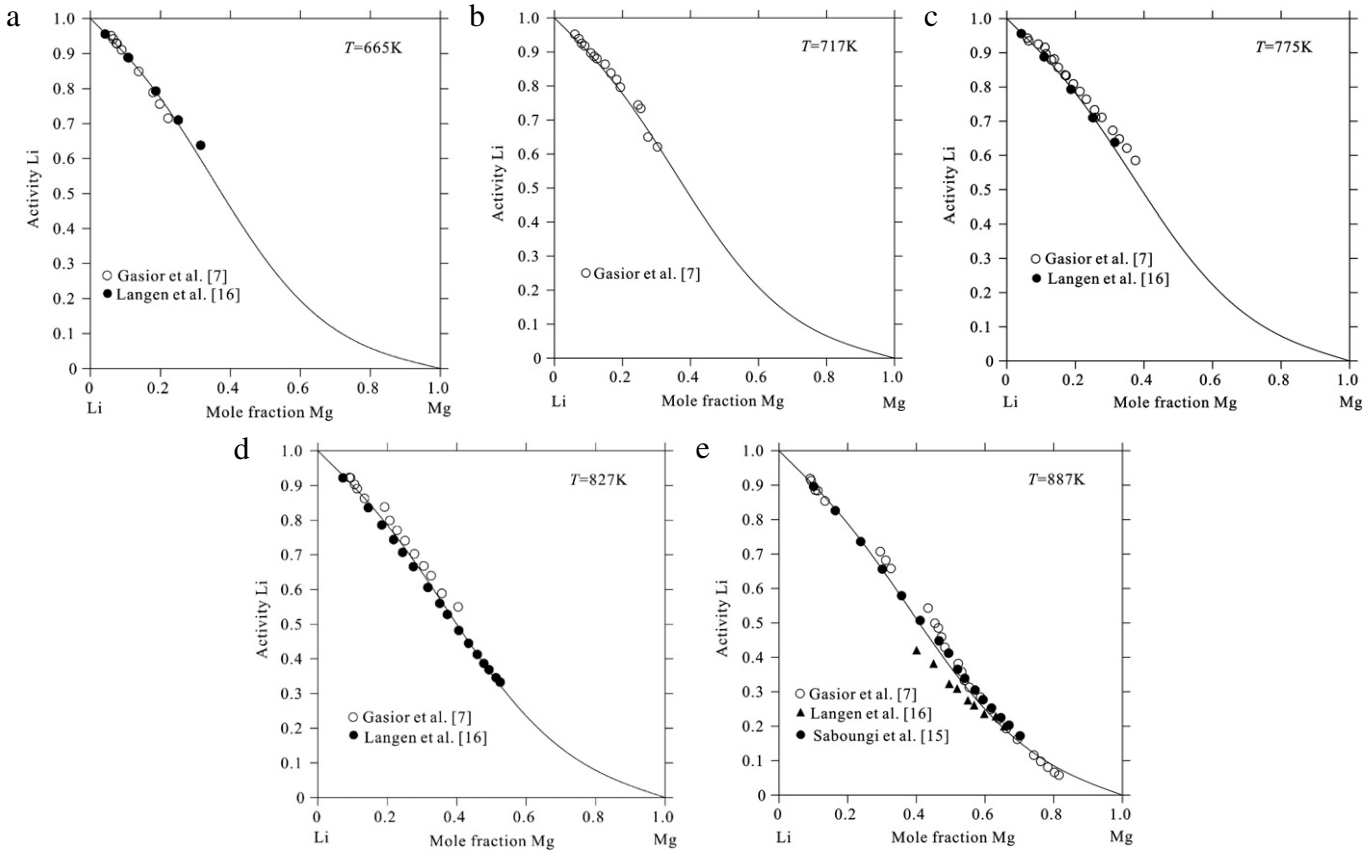

Fig. 5. Calculated activities of Li in liquid phase along with experimental data [7,15,16] (a) at 665 K (b) at 717 K (c) at 775 K (d) at 827 K (e) at 887 K.

4.2. The Al–Li–Mg system

The advantage of CALPHAD modeling is to predict phase diagrams and thermodynamic properties of the higher order systems with some certainties by means of thermodynamic extrapolation. Thus the calculated phase stabilities beyond experimental results are very important. Allowing for this, after the optimization, we first checked the phase stabilities of the present calculation to see whether some artificial phase relations, such as inverse miscibility gap and restability of compounds, emerge at high temperatures. A series of isothermal sections were calculated from 1000 to 4000 °C with an interval of 500 °C. It shows that the present calculation is stable below 3500 °C. However, above 3500 °C, the AlLi phase restabilizes at the Li–Mg side. The reason for the restability of the AlLi phase at high temperature is that the parameter b of $G^{AlLi}_{Mg:Li}$ is too negative. It can be eliminated by imposing a constraint to guarantee a negative value for the driving force of the AlLi phase above 3500 °C, as described by Wang et al. [38]. However, at such high temperature, gas is stable instead of the liquid phase. Thus, the present calculation is acceptable. The optimized parameters of the Al–Li–Mg system are listed in Table 2.

The enthalpies of mixing for liquid phases [31] were used to obtain the preliminary ternary parameters for the liquid phase. Three ternary parameters ${}^{0}L^{L}_{Al,Li,Mg}$ ${}^{1}L^{L}_{Al,Li,Mg}$ and ${}^{2}L^{L}_{Al,Li,Mg}$ are indispensable to describe these data. The calculated enthalpies of mixing for liquid phases along various composition sections at 955 K are shown in Figs. 9–12. It is demonstrated that these experimental data [31] are well described by the present thermodynamic calculation. It should be emphasized that the parameter ${}^{1}L^{L}_{Al,Li,Mg}$ is assessed with a value of about −50,000 for

Table 2
Summary of the assessed thermodynamic parameters in the Al–Li–Mg system.

(I) The binary phases in the Li–Mg system
Phase: liquid model: (Al, Li, Mg)
$^0L^{L}_{Li,Mg} = -13172 - 4.3009 \cdot T$
$^1L^{L}_{Li,Mg} = -1912 + 2.7115 \cdot T$
$^2L^{L}_{Li,Mg} = 2531$

Phase: (Li) model: $(Li, Mg, Va)_1(Va)_3$
$^0L^{(Li)}_{Li,Mg:Va} = -13329 - 2.2478 \cdot T$
$^1L^{(Li)}_{Li,Mg:Va} = 2597$
$^2L^{(Li)}_{Li,Mg:Va} = 1077 + 3.3872 \cdot T$
$^0L^{(Li)}_{Li,Va:Va} = 350,000$
$^0L^{(Li)}_{Mg,Va:Va} = 350,000$

Phase: (Mg) model: $(Li, Mg)_1(Va)_{0.5}$
$^0L^{(Mg)}_{Li,Mg:Va} = 4743 - 9.2722 \cdot T$
$^1L^{(Mg)}_{Li,Mg:Va} = -2395$

(II) The ternary phases in the Al–Li–Mg system
Phase: liquid model: (Al, Li, Mg)
$^0L^{L}_{Al,Li,Mg} = 2341 - 38.9356 \cdot T$
$^1L^{L}_{Al,Li,Mg} = -51293 + 29.7042 \cdot T$
$^2L^{L}_{Al,Li,Mg} = -11268 + 30.0684 \cdot T$

Phase: (Mg) model: $(Al, Li, Mg)_1(Va)_{0.5}$
$^0L^{(Mg)}_{Al,Li,Mg:Va} = 36,368$
$^1L^{(Mg)}_{Al,Li,Mg:Va} = -41,076$
$^2L^{(Mg)}_{Al,Li,Mg:Va} = -86,738 + 76.9259 \cdot T$

Phase: (Li) model: $(Al, Li, Mg)_1(Va)_3$
$^0L^{(Li)}_{Al,Li,Mg:Va} = -21460$
$^1L^{(Li)}_{Al,Li,Mg:Va} = -143581 + 22.4205 \cdot T$
$^2L^{(Li)}_{Al,Li,Mg:Va} = -2114$

Phase: (Al) model: $(Al, Li, Mg)_1(Va)_1$
$^0L^{(Al)}_{Al,Li,Mg:Va} = -47,954 - 91.1362 \cdot T$
$^1L^{(Al)}_{Al,Li,Mg:Va} = 283,196$
$^2L^{(Al)}_{Al,Li,Mg:Va} = 141,819$

Phase: AlLi model: $(Al, Li, Mg)_{0.5}(Li, Mg, Va)_{0.5}$
$G^{AlLi}_{Mg:Li} - G^{(Mg)}_{Mg} - G^{(Li)}_{Li} = 8322 - 13.8490 \cdot T$
$G^{AlLi}_{Al:Mg} - G^{(Al)}_{Al} - G^{(Mg)}_{Mg} = 12,110 - 14.0353$
$G^{AlLi}_{Li:Mg} - G^{(Li)}_{Li} - G^{(Mg)}_{Mg} = 32,133$
$G^{AlLi}_{Mg:Mg} - 2 \cdot G^{(Mg)}_{Mg} = 13,958$
$G^{AlLi}_{Mg:Va} - G^{(Mg)}_{Mg} = 75,193$
$^0L^{AlLi}_{Al,Mg:Li} = -6418 + 1.9934 \cdot T$
$^0L^{AlLi}_{Al:Mg,Li} = -21,782 + 22.9291 \cdot T$

Phase: γ model: $(Li, Mg)_{10/58}(Al, Mg)_{24/58}(Al, Mg)_{24/58}$
$G^{\gamma}_{Li:Al:Al} - 10/58 \cdot G^{(Li)}_{Li} - 48/58 \cdot G^{(Al)}_{Al} = 5197 - 12.4014 \cdot T$
$G^{\gamma}_{Li:Mg:Al} - 10/58 \cdot G^{(Li)}_{Li} - 24/58 \cdot G^{(Mg)}_{Mg} - 24/58 \cdot G^{(Al)}_{Al} = -13,540 + 6.7766 \cdot T$
$G^{\gamma}_{Li:Al:Mg} - 10/58 \cdot G^{(Li)}_{Li} - 24/58 \cdot G^{(Al)}_{Al} - 24/58 \cdot G^{(Mg)}_{Mg} = 12,120$
$G^{\gamma}_{Li:Mg:Mg} - 10/58 \cdot G^{(Li)}_{Li} - 48/58 \cdot G^{(Mg)}_{Mg} = 12,301$
$^0L^{\gamma}_{Li,Mg:Mg:Al} = -3730 + 6.2861 \cdot T$

Phase: β model: $Al_{140/229}(Li, Mg)_{89/229}$
$G^{\beta}_{Al:Li} - 140/229 \cdot G^{(Al)}_{Al} - 89/229 \cdot G^{(Li)}_{Li} = -6331$
$^0L^{\beta}_{Al:Mg:Li} = -11,077 + 7.4224 \cdot T$

Phase: Al_2Li_3 model: $(Al, Mg)_{0.4}Li_{0.6}$
$G^{Al_2Li_3}_{Mg:Li} - 0.4 \cdot G^{(Mg)}_{Mg} - 0.6 \cdot G^{(Li)}_{Li} = 2150$
$^0L^{Al_2Li_3}_{Al,Mg:Li} = -8294$

Phase: τ model: $Al_{0.53}Li_{0.33}Mg_{0.14}$
$G^{\tau}_{Al:Li:Mg} - 0.53 \cdot G^{(Al)}_{Al} - 0.33 \cdot G^{(Li)}_{Li} - 0.14 \cdot G^{(Mg)}_{Mg} = -14,681 + 2.9211 \cdot T$

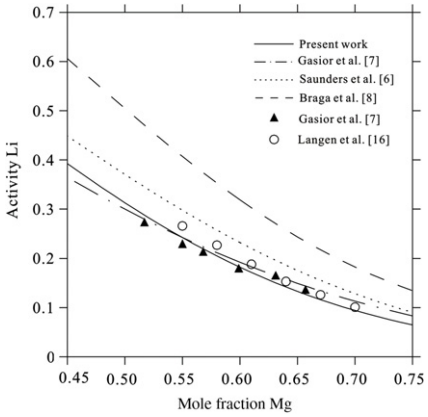

Fig. 6. Calculated activity of Li in (Li) at 806 K resulting from Gasior et al. [7], Saunders [6], Braga et al. [8] and the present work along with the experimental data [7,16].

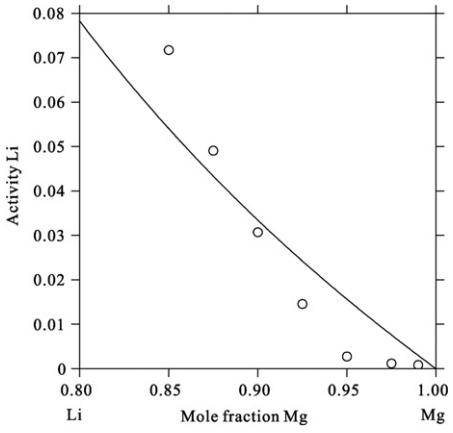

Fig. 7. Calculated activity of Li in (Mg) at 700 K along with the experimental data [7].

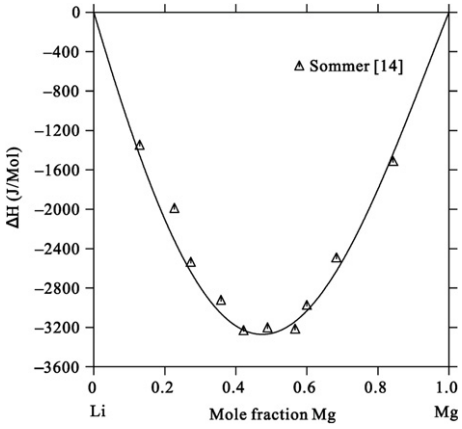

Fig. 8. Calculated enthalpies of mixing for liquid phase at 667 °C compared with the experimental data [14].

a good description for the enthalpies of mixing of liquid phases. In the next part, the noticeable effects of this parameter on the phase equilibria of the liquid phase, especially at the Li-rich corner, will be discussed.

Fig. 13 shows a good consistency between the calculated isothermal sections at 200, 300, 400 °C and the experimental data. It is found that the calculated liquid phase region in the Li-rich corner is much larger than the assessed results of Ghosh [17]. As has been mentioned above, a very large negative value for $^1L^{L}_{Al,Li,Mg}$

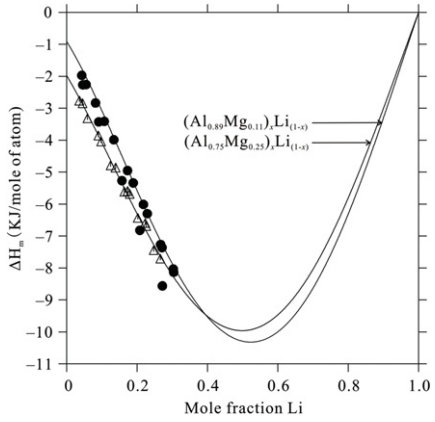

Fig. 9. Calculated enthalpies of mixing of liquid at 955 K along the two composition sections $(Al_{0.75}Mg_{0.25})_xLi_{(1-x)}$, $(Al_{0.89}Mg_{0.11})_xLi_{(1-x)}$. □ and • denote the experimental data along the section $(Al_{0.75}Mg_{0.25})_xLi_{(1-x)}$, $(Al_{0.89}Mg_{0.11})_xLi_{(1-x)}$, respectively [31].

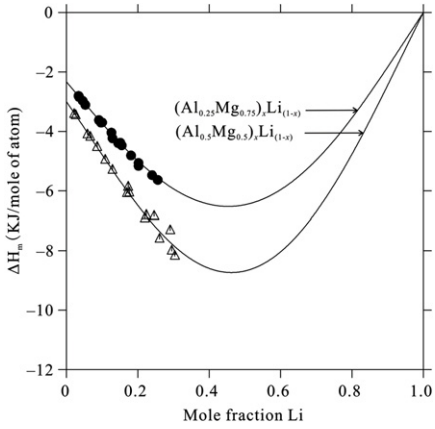

Fig. 10. Calculated enthalpies of mixing of liquid at 955 K along two composition sections $(Al_{0.5}Mg_{0.5})_xLi_{(1-x)}$, $(Al_{0.25}Mg_{0.75})_xLi_{(1-x)}$. □ and • denote the experimental data along the section $(Al_{0.5}Mg_{0.5})_xLi_{(1-x)}$, $(Al_{0.25}Mg_{0.75})_xLi_{(1-x)}$, respectively [31].

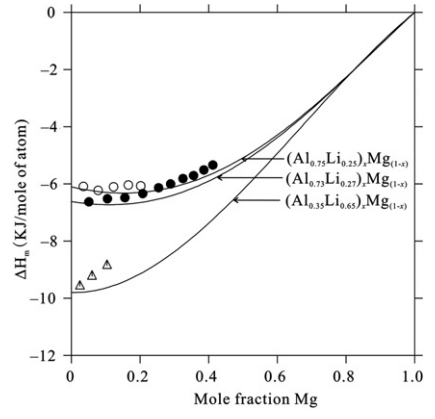

Fig. 11. Calculated enthalpies of mixing of liquid at 955 K along the composition sections $(Al_mLi_n)_xMg_{(1-x)}$. □ • ○ denote the experimental data along the section $(Al_{0.35}Li_{0.65})_xMg_{(1-x)}$, $(Al_{0.73}Li_{0.27})_xMg_{(1-x)}$, $(Al_{0.75}Li_{0.25})_xMg_{(1-x)}$, respectively [31].

is evaluated considering the thermodynamic data. Consequently, the presently calculated liquid phase is more stable than the one by direct thermodynamic extrapolation. As a result, the present calculated liquid phase region is much larger than the assessed results of Ghosh [17]. Considering the fact that the assessed results of Ghosh [17] are based only on the phase equilibrium data, the present results are much more reasonable.

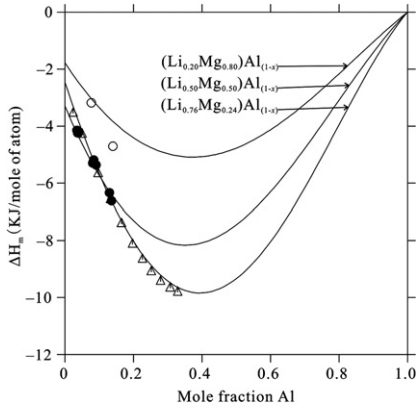

Fig. 12. Calculated enthalpies of mixing of liquid at 955 K along the composition sections $(Li_mMg_n)_xAl_{(1-x)}$. □ • ○ denote the experimental data along the section $(Li_{0.76}Mg_{0.24})_xAl_{(1-x)}$, $(Li_{0.50}Mg_{0.50})_xAl_{(1-x)}$, $(Li_{0.20}Mg_{0.80})_xAl_{(1-x)}$, respectively [31].

The calculated 5 vertical sections along various compositions compared with the experimental data [10] are shown in Fig. 14. As mentioned above, the liquidus data in the Li-rich region were given lower weight because these data are less accurate [7]. Therefore, the calculated liquidus in the Li-rich region shows considerable deviations from the experimental data, as shown in Fig. 14(b). Except for these deviations, the other experimental data are well reproduced by the present modeling.

Table 3 presents the comparison between the calculated invariant reactions and experimental data. The calculated liquidus surface projection is shown in Fig. 15. The reaction scheme associated with the liquid phase, which is important for practical applications, is presented in Fig. 16. The invariant reactions can be well reproduced using the present thermodynamic parameters. The agreement between the calculated temperatures and compositions for the invariant reactions and the experimental ones are fairly well within the experimental errors. However, further discussions are needed for the U_4 reaction. As can be seen from Figs. 15 to 16, the reaction type will change to eutectic if the temperature is decreased just 2 °C to the temperature below 450 °C. On the other hand, if the temperature is increased just 2 °C to the temperature above 452 °C, the reaction will be a peritectic one. However, it should be stated that the error of the measurement for the invariant reaction temperature is greater than 9 °C as has been pointed out by Ghosh [17]. So it is hard to judge which result [4,10] is right only based on these experimental information. The calculation by using the obtained thermodynamic parameters in this work shows the reaction is a transition type one, which is consistent with the work by Schürmann and Voss [10]. The reliability of the present calculation can be validated by the three maximum points in the present calculation. As shown in Fig. 15, there are three maximum points $p_{1,\max}$, $e_{3,\max}$ and $e_{4,\max}$. The calculated temperatures of the three maximum points are 545, 480 and 476 °C respectively, which are in good agreement with the assessed temperatures (545, 485 and 480 °C) [17] based on the measurement [10]. It should be mentioned here that the three assessed temperatures [17] were not used during optimization. Thus, the consistency between our calculation and the assessment [17] provides another evidence on the reliability of the present calculation.

In the Li-rich corner without experimental data, the present calculation shows that Al_4Li_9 is formed by a transition reaction $L + Al_2Li_3 = Al_4Li_9 + (Li)$ at 195 °C, which is much lower than the assessed temperature 350 °C by Ghosh [17]. And this is also due to the large negative value of ${}^1L^L_{Al,Li,Mg}$.

5. Conclusions

Taking into account the latest experimental data, the Li–Mg binary system has been re-assessed in the present work. The

Table 3
The calculated invariant reactions in this work compared with the reported results [4,10].

Reaction (type)	Temperature (°C)	Phase	Composition, at.%			Source
			Al	Li	Mg	
$L + \mathrm{AlLi} = (\mathrm{Al}) + \tau$ (U_1)	536	L	66.0	19.4	14.6	[10]
		AlLi	53.5	40.7	5.8	
		(Al)	81.5	12.0	6.5	
		τ	54.2	34.5	11.3	
	528	L	66.1	16.7	17.2	[4]
	524	L	64.9	19.9	15.2	This work
		AlLi	52.6	42.0	5.4	
		(Al)	81.6	11.6	6.8	
		τ	53.0	33.0	14.0	
$L + \tau = (\mathrm{Al}) + \gamma$ (U_2)	483	L	61.5	10.8	27.7	[10]
		τ	54.5	31.0	14.5	
		(Al)	79.3	8.4	12.3	
		γ	48.3	16.4	35.3	
	485	L	63.4	12.1	24.5	[4]
	475	L	60.6	12.7	26.7	This work
		τ	53.0	33.0	14.0	
		(Al)	79.7	8.2	12.1	
		γ	57.8	14.3	27.9	
$L + \tau = \mathrm{AlLi} + \gamma$ (U_3)	464	L	39.8	20.1	40.1	[10]
		τ	51.2	34.4	14.4	
		AlLi	45.5	40.8	13.7	
		γ	42.5	18.6	38.7	
	463	L	37.2	20.8	42.0	This work
		τ	53.0	33.0	14.0	
		AlLi	47.2	38.8	14.0	
		γ	44.5	15.9	39.6	
$L + (\mathrm{Al}) + \gamma = \beta$ (U_4)	458	L	60.5	6.0	33.5	[10]
		(Al)	80.7	2.9	16.4	
		γ	51.9	10.7	37.4	
		β	60.5	7.2	32.3	
	451	L	61.0	5.4	33.6	This work
		(Al)	79.6	5.0	15.4	
		γ	55.5	9.1	35.4	
		β	61.1	5.4	33.5	
$L + (\mathrm{Li}) = (\mathrm{Mg}) + \mathrm{AlLi}$ (U_5)	436	L	23.9	29.3	46.8	[10]
		(Li)	0.2	37.5	62.3	
		(Mg)	7.9	20.2	71.9	
		AlLi	39.5	44.5	16.5	
	431	L	22.1	27.6	50.2	This work
		(Li)	11.4	29.2	59.4	
		(Mg)	8.9	18.5	72.6	
		AlLi	41.6	43.7	14.7	
$L = (\mathrm{Mg}) + \gamma + \mathrm{AlLi}$ (E_1)	418	L	19.0	20.6	50.4	[10]
		(Mg)	10.2	12.6	76.2	
		γ	37.7	17.7	44.6	
		AlLi	41.6	42.5	15.9	
	425	L	25.5	22.9	51.6	This work
		(Mg)	10.4	14.6	75.0	
		γ	42.1	16.4	41.5	
		AlLi	43.9	41.3	14.8	
$L + \mathrm{AlLi} = \mathrm{Al_2Li_3} + (\mathrm{Li})$ (U_6)	411	L	12.6	61.0	26.4	[10]
		AlLi	39.4	50.5	10.1	
		$\mathrm{Al_2Li_3}$	30.5	67.5	2.3	
		(Li)	0.2	63.0	36.8	
	403	L	12.5	64.0	23.5	This work
		AlLi	36.1	52.6	11.3	
		$\mathrm{Al_2Li_3}$	32.9	60.0	7.1	
		(Li)	8.6	58.0	33.4	
$L + \mathrm{Al_2Li_3} = \mathrm{Al_4Li_9} + (\mathrm{Li})$ (U_7)	195	L	2.2	93.1	4.7	This work
		$\mathrm{Al_2Li_3}$	34.5	60.0	54.5	
		$\mathrm{Al_4Li_9}$	30.8	69.2	0.	
		(Li)	1.2	89.1	9.7	

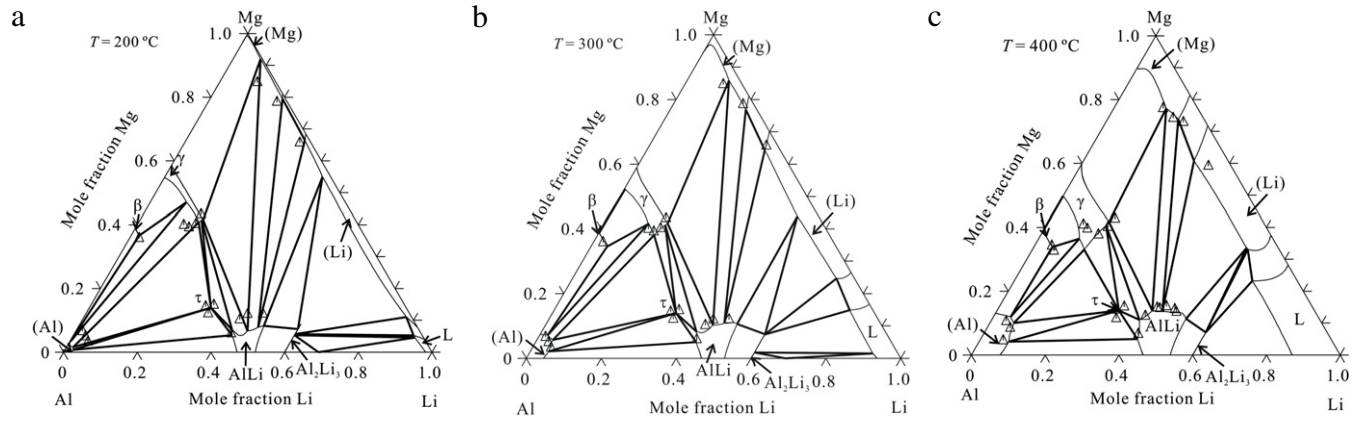

Fig. 13. Calculated isothermal sections at (a) 200 °C (b) 300 °C and (c) 400 °C, compared with the experimental data [27], respectively.

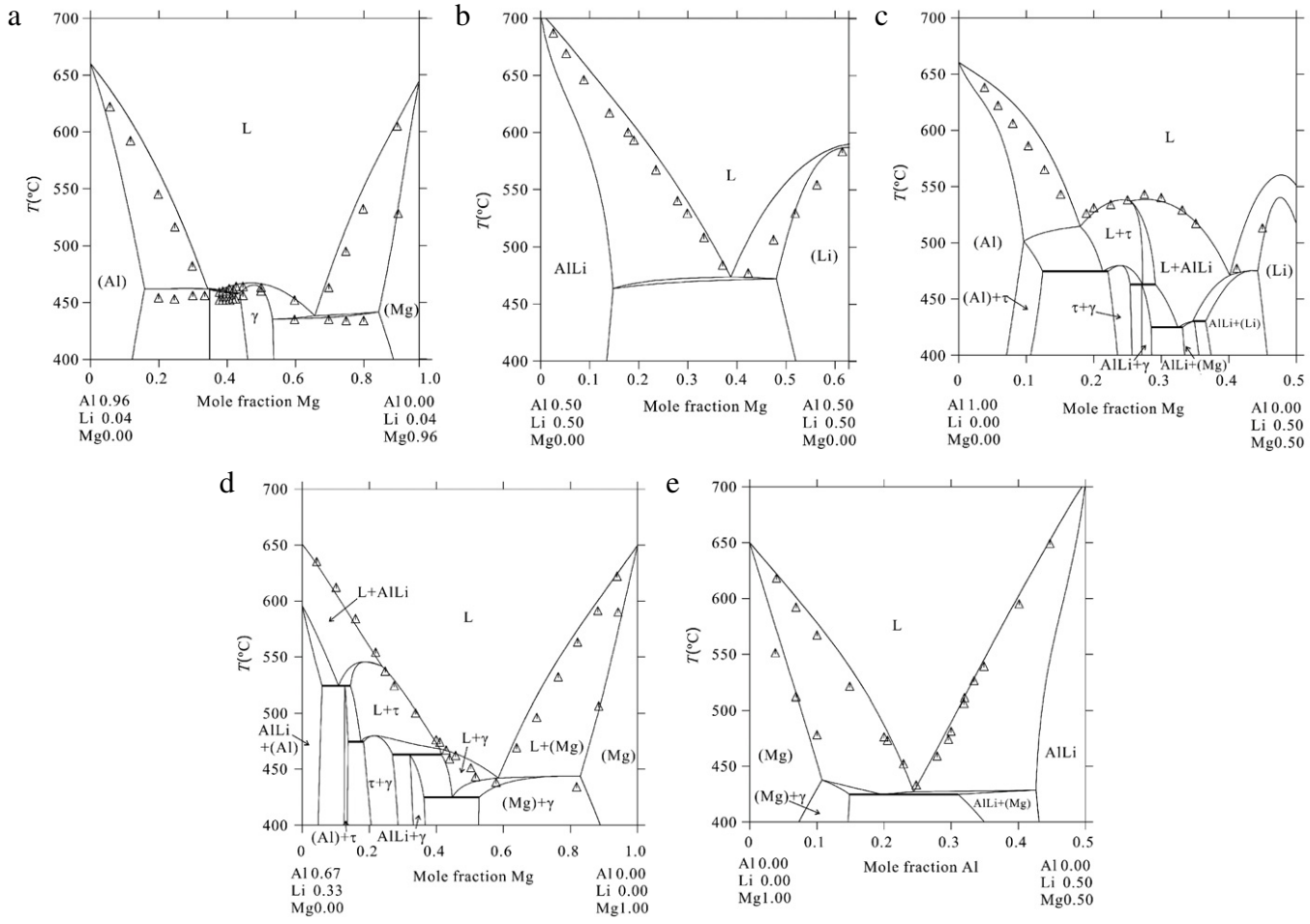

Fig. 14. Calculated vertical sections along various compositions compared with the experimental data [10] (a) for $x(\mathrm{Li}) = 0.04$, (b) for $126 \cdot x(\mathrm{Li}) + 26 \cdot x(\mathrm{Mg}) = 63$, (c) for $x(\mathrm{Li}) = x(\mathrm{Mg})$, (d) for $x(\mathrm{Al}) - 2 \cdot x(\mathrm{Li}) = 0$, (e) for $x(\mathrm{Al}) = x(\mathrm{Li})$.

presently calculated phase diagram and thermodynamic properties can reproduce the experimental data reasonably. The artificial phase equilibria existing in the previous optimizations [7,8] have been eliminated. Based on the obtained thermodynamic description for the Li–Mg system in the present work and those for Al–Li and Al–Mg in the literature, the Al–Li–Mg system has been briefly reviewed. And a thorough thermodynamic modeling of the Al–Li–Mg system over the entire compositional and temperature ranges has been conducted based on selected experimental data. A set of self-consistent thermodynamic parameters for the Al–Li–Mg system has been obtained. Comparisons between the calculated and experimental results in the Al–Li–Mg system show that the present description can account for the experimental data satisfactorily.

Acknowledgments

The present authors are grateful to Prof. Z. Moser in the Institute of Metallurgy and Materials Science, Polish Academy of Sciences, for his help in the assessment of Li–Mg system. The financial

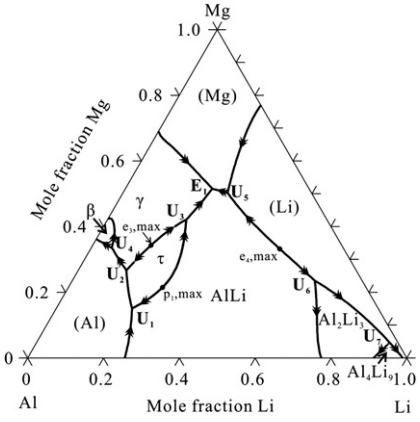

Fig. 15. Calculated liquidus surface projection of the Al–Li–Mg system.

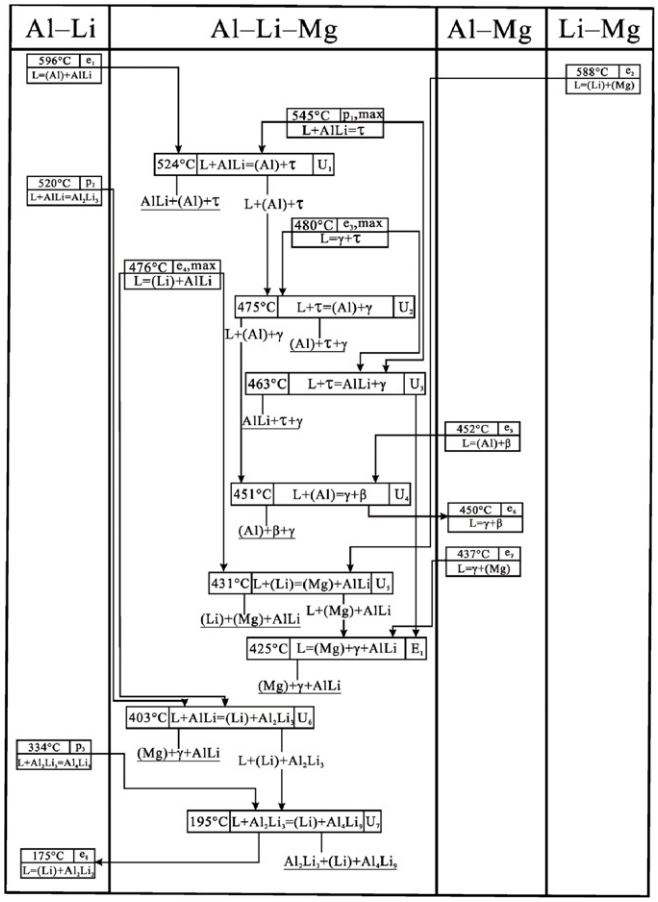

Fig. 16. Scheil reaction scheme of the Al–Li–Mg system.

support from the Key Program of the National Natural Science Foundation of China (Grant No. 50831007), the Creative Research Group of National Natural Science Foundation of China (Grant No. 51021063) and the National Natural Science Foundation of China (Grant No. 51071179) is greatly acknowledged.

Appendix. Supplementary data

Supplementary material related to this article can be found online at doi:10.1016/j.calphad.2011.09.003.

References

[1] H.E. Friedrich, B.L. Mordike, Magnesium Technology, Springer-Verlag, Berlin Heidelberg, 2006.
[2] Z. Chen, Magnesium Alloys, Chemical Industry Press, Beijing, 2004.
[3] L.S. Kramer, T.J. Langan, J.R. Pickens, H. Last, J. Mater. Sci. 29 (1994) 5826–5832.
[4] B. Dubost, P. Bompard, I. Ansara, J. Phys. C3 (1987) 473–479.
[5] N. Saunders, Z Metallkd. 80 (1989) 894–903.
[6] N. Saunders, CALPHAD 14 (1990) 61–70.
[7] W. Gasior, Z. Moser, W. Zakulski, G. Schwitzgebel, Metall. Mater. Trans. A 27A (1996) 2419–2428.
[8] M.H. Braga, L.F. Malheiros, M. Hämäläinen, Thermochim. Acta. 344 (2000) 47–54.
[9] A.A. Nayeb-Hashemi, J.B. Clark, A.D. Pelton, Bull. Alloy Phase Diagrams 5 (1984) 365–374.
[10] E. Schürmann, H.-J. Voss, Giessereiforschung 33 (1981) 33–52.
[11] J.A. Rowland, Jr.C.E. Armantrout, D.F. Walsh, Trans. AIME, J. Met. 203 (1955) 355–359.
[12] W. Hume-Rothery, G.V. Raynor, E. Butchers, J. Inst. Met. 71 (1945) 589–601.
[13] J.A. Catteral, Nature 169 (1952) 336.
[14] F. Sommer, Z Metallkd. 70 (1979) 359–361.
[15] M.-L. Saboungi, M. Blander, J. Eleetrochem. Sot. 122 (1975) 1631–1634.
[16] G. Langen, G. Schwitzgebel, H. Ruppersberg, Mat. Res. Bull. 19 (1984) 1141–1147.
[17] G. Ghosh, in: Landolt–Bornstein, Group IV, Physical Chemistry, Berlin Heidelberg, 2005.
[18] A.J. McAlister, Bull. Alloy Phase Diagrams 3 (1982) 177–183.
[19] S.G.T.E. SGTE, in: Landolt–Bornstein, Group IV, Physical Chemistry, Berlin Heidelberg, 2002.
[20] F.I. Shamray, Izv. Akad. Nauk. SSSR, Otdel. Khim. Nauk. (1948) 290–301.
[21] M.E. Drits, E.M. Padezhnova, L.S. Guzei, Izv. Akad. Nauk. SSSR, Met. (1977) 205–209.
[22] A. Jones, J.H. Lennon, R.R. Nash, W.H. Chang, E.G. Macpeek, US At Energy Comm. Publ. (1952) 1–130.
[23] A.F. Weinberg, D.W. Levison, D.J. McPherson, W. Rostoker, C.P. Wolfe, A. Humphreys, J. Dvorak, H. Manasevit, W. DuPraw, Armour Res. Found Rep. (1954) 1–94.
[24] D.W. Levison, D.J. McPherson, Trans. Am. Soc. Met. 48 (1956) 689–697.
[25] M.E. Drits, E.S. Kadaner, N.I. Turkina, V.I. Kuz'mina, Izv. Akad. Nauk. SSSR, Met. (1973) 225–229.
[26] E.M. Padezhnova, E.V. Melmik, L.S. Guzei, L.N. Guseva, Izv. Akad. Nauk. SSSR, Met. (1976) 222–226.
[27] E. Schürmann, I.K. Geissler, Giessereiforschung 32 (1980) 163–174.
[28] F.I. Shamray, N.S. Kurnakov, Bull. Acad. Sci. URSS, Classe Sci. Chim. (1948) 83–94.
[29] G.E. Thompson, B. Noble, J. Inst. Met. 101 (1973) 111–115.
[30] L.V. Nikulin, S.B. Shevrikuko, E.V. Belozerova, Tsvetn. Met. (1985) 56–59.
[31] Z. Moser, R. Agarwal, F. Sommer, B. Predel, Z Metallkd. 82 (1991) 317–321.
[32] A.T. Dinsdale, CALPHAD 15 (1991) 317–425.
[33] O. Redlich, A.T. Kister, Indust. Eng. Chem. 40 (1948) 345–348.
[34] P. Liang, H.L. Su, P. Donnadieu, M.G. Harmelin, A. Quivy, P. Ochin, G. Effenberg, H.J. Seifert, H.L. Lukas, F. Aldinger, Z Metallkd. 89 (1998) 536–540.
[35] B. Sundman, J. Ågren, J. Phys. Chem. Solids 42 (1981) 297–301.
[36] B. Sundman, B. Jansson, J.-O. Andersson, CALPHAD 9 (1985) 153–190.
[37] Y. Du, R. Schmid-Fetzer, H. Ohtani, Z Metallkd. 88 (1997) 545–556.
[38] P. Wang, L. Zhou, Y. Du, H. Xu, S. Liu, L. Chen, Y. Ouyang, J. Alloys Compd. 509 (2011) 2679–2683.